Why $Pb(B,B')O_3$ Perovskites Disorder at Lower Temperatures than $Ba(B,B')O_3$ Perovskites

B.P. Burton and E. Cockayne
Materials Science and Engineering Laboratory, Ceramics Division, National Institute of Standards and Technology, Gaithersburg, MD 20899
(September 26, 2002)
Published in Physical Review **B60** R12 542- (1999)

Abstract

Planewave pseudopotential calculations of total energies were performed for three ordered perovskite related supercells in each of the eight stoichiometries of $A(B_{1/3}B'_{2/3})O_3$; $A = Pb,\ Ba$ and $B = Zn,\ Mg$ and $B' = Nb,\ Ta$; and the eight stoichiometries of $A(B_{1/2}B'_{1/2})O_3$; $B = Sc,\ In$. A striking difference between the Pb- and $Ba(B_{1/3}B'_{2/3})O_3$ systems is that the differences in total energies for Pb-systems span ranges that are roughly an order of magnitude smaller than those for the corresponding Ba-systems. This indicates much lower energetic barriers to disordering in the Pb-systems, consistent with experiments. We explain this trend as a consequence of enhanced $Pb-O$ bonding to underbonded oxygens in $B^{2+}-O-B^{2+}$ environments.

Accepted for Rapid publication in Phys. Rev. B, Octtober 1999

PACS Numbers: 64.60.Cn, 81.30.-t, 77.84.-s

I. INTRODUCTION

Lead based $A(B,B')O_3$ perovskites ($A = Pb^{2+}, Ba^{2+}$; $B = Mg^{2+}, Zn^{2+}, In^{3+}, Sc^{3+}$; $B' = Nb^{5+}, Ta^{5+}$) are widely used as relaxor ferroelectric[1,2] transducers, actuators, and multilayer capacitors; and their $Ba(B,B')O_3$ counterparts, particularly $Ba(Zn_{1/3}Ta_{2/3})O_3$, are the premier dielectric resonator materials[3]. Some $B-site$ disorder is essential to obtain the relaxor properties of the Pb-systems[1,2], but disorder in the Ba-systems can degrade the dielectric "quality factor" by orders of magnitude[4,5]. As indicated by the experimental data summarized in Table 1, $B-site$ ordering in $A(B,B')O_3$ perovskites persists to higher temperatures when the $A-cation$ is Ba^{2+} rather than Pb^{2+}, especially in the $A(B_{1/3}B'_{2/3})O_3$ systems[4,6–8,10–13]. Clearly, the energetics of $B-site$ ordering are dramatically altered by substituting Pb for Ba on the $A-sites$, and it is not obvious why this should occur. Our computational results allow us to explain this surprizing result as a consequence of enhanced $Pb-O$ hybridization between the Pb $6s$- and O $2p$-states of *underbonded oxygens* in $B^{2+}-O-B^{2+}$ or $B^{2+}-O-B^{2+}$ environments.

All the $Ba(B_{1/3}B'_{2/3})O_3$ systems, adopt the same $1:2$ crystal structure at low temperatures (a $B:B':B'$ layer sequence perpendicular to the cubic [111] vector) but the only $Pb(B_{1/3}B'_{2/3})O_3$ system, that exhibits long range order is $Pb(Mg_{1/3}Ta_{2/3})O_3$. When maximally ordered, the PMT $1:1$ structure, has two $B-sites$: one occupied by Ta; the other by a disordered $Mg_{2/3}Ta_{1/3}$ mixture. Thus, $1:1$ is a partially ordered intermediate temperature phase rather than the PMT ground state (GS). In the $A(B_{1/2},B'_{1/2})O_3$ systems, all stoichiometries adopt a $1:1$ structure at low temperatures, and again the $Ba(B_{1/2},B'_{1/2})O_3$ systems have higher transition temperatures for cation ordering[10,14,19].

II. TOTAL ENERGY CALCULATIONS

Total energies were calculated for three fifteen-atom perovskite based superstructures in each of the eight possible stoichiometries of $A(B_{1/3}B'_{2/3})O_3$; $A = Pb,\ Ba$ $B = Mg,\ Zn$ $B' = Nb,\ Ta$ (Fig. 1). The three $A(B_{1/3}B'_{2/3})O_3$ superstructures ($[111]_{1:2}$, $[110]_{1:2}$, and $[001]_{1:2}$) are derived from ideal perovskite by adding a $(B:B':B')$ layer sequence perpendicular to the [111], [110], and [001] cubic vectors, respectively. , The three ten-atom $A(B_{1/2}B'_{1/2})O_3$ superstructures, $[111]_{1:1}$, $[110]_{1:1}$, and $[001]_{1:1}$, are derived by adding $B:B'$ layer sequences perpendicular to the [111], [110], and [001] cubic vectors. All calculations were performed with the Vienna *ab initio* simulation program (VASP)[23] using ultrasoft Vanderbilt[24] type plane-wave pseudopotentials with a local density approximation for exchange and correlation energies. Electronic degrees of freedom were optimized with a conjugate gradient algorithm, and both cell constant and ionic positions were fully relaxed, but ferroelastic acentric relaxations were not investigated. Valence electron configurations for the pseudopotentials are: Pb $5d^{10}6p^26s^2$ (Pb_d version); Ba $5p^66s^2$; Mg $2p^63s^2$; Zn $3d^{10}4s^2$; Sc $3p^63d4s^2$; In $4d^{10}5s^25p^1$; Nb $4p^65s4d^4$; Ta $5d^36s^2$; O $2p^6$. An energy cutoff of 395.7 eV was used, in the "high precision" option which guarantees that *absolute* energies are converged to within a few meV (a few tenths of kJ/mol; mol = ABO_3). To promote cancellation of errors, formation energies for the ABO_3 and $AB'O_3$ reference states, are calculated for each supercell with identical K-point meshes: 5x5x4, 4x4x10, and 6x6x2 for $[111]_{1:2}$, $[110]_{1:2}$,

and $[001]_{1:2}$ superstructures, respectively; 4x4x4, 7x7x10, and 8x8x4 for $[111]_{1:1}$, $[110]_{1:1}$, and $[001]_{1:1}$, respectively.

VASP results for $A(B_{1/3}B'_{2/3})O_3$ supercell total energies, relative to $E_{[111]_{1:2}}$, are plotted in Figure 1 with the corresponding supercell energies calculated with the ionic model of Bellaiche and Vanderbilt (BV)[25], in which:

$$E = \frac{e^2}{2\epsilon a}\sum_{l\neq l'}\frac{\Delta q_l \Delta q_{l'}}{|l-l'|} \qquad (1)$$

Where: E is total energy; e is the electron charge; ϵ is an electronic dielectric constant ($\epsilon = 10$ for $A(B_{1/3}B'_{2/3})O_3$, $\epsilon = 5$ for $A(B_{1/2}B'_{1/2})O_3$); a is the lattice constant ($a = 7.7$ $a.u., 4.07$ $\mathring{A}$)[26]; Δq_l is the difference in charge between the ion at site l and the average $B-site$ charge of +4; i.e. $\Delta q_l = -2$ for Mg^{2+} and $+1$ for Nb^{5+}; $a|l-l'|$ is the interionic separation. For the $A(B_{1/3}B'_{2/3})O_3$ composition, this model predicts a $1:2$ GS and a $1:2 \rightleftharpoons Disordered$ transition at high temperature, consistent with the experimental data for the $Ba(B_{1/3}B'_{2/3})O_3$ systems.

In Figs. 1 and 2, the BV (ionic) model values and all the Ba-systems, exhibit the same hierarchies: $\Delta E_{[111]_{1:2}} < \Delta E_{[110]_{1:2}} < \Delta E_{[001]_{1:2}}$. In the Pb-systems, however, this hierarchy only occurs in PMN and PZT. Experimentally, the $1:2$ structure ($[111]_{1:2}$) is observed as the low temperature, presumably GS phase for all the Ba-systems, and it is the predicted GS of the BV model. In the Pb-systems however, the $1:2$ structure may not be the GS for any of them; in PMN for example, at least one 30 atom superstructure is predicted to have lower energy[27]. Energy ranges, $\Delta E_{[001]_{1:2}} - \Delta E_{[001]_{1:2}}$, for the BV values and the Ba-systems, are between 40 and 60 kJ/mol (mol = ABO_3), but analogous ranges for the Pb-systems, $\Delta E_{highest} - \Delta E_{lowest}$ are between 1 and 8 kJ/mol. In $A(B_{1/2}B'_{1/2})O_3$ systems (Fig. 2), ΔE-ranges for the Pb-systems are about half of those for the Ba-systems. A second trend that occurs in both Figs. 1 and 2 is that ΔE-ranges for $A(B,Nb)O_3$ systems are typically a little smaller than those for the corresponding $A(B,Ta)O_3$ systems; consistent with experimental data indicating higher transition temperatures for cation ordering in Ta-systems (Table 1).

III. DISCUSSION

The configurational energy is apparently dominated by two contributions: long-range Coulomb interactions which favor configurations that maximize unlike charges on nearest neighbor $B-sites$; and short-range interactions that are primarily associated with the optimization of $A-O$ bonds. Long-range electrostatic interactions dominate when the $A-cation$ is the larger more regularly coordinated Ba^{2+}, and short-range interactions become competitive when it is the smaller less regularly coordinated Pb^{2+}.

Concentrations of underbonded oxygens in $B^{2+}-O-B^{2+}$ or $B^{3+}-O-B^{3+}$ environments increase monotonically in the sequences of structures $[111]_{1:2}$, $[110]_{1:2}$, and $[001]_{1:2}$

(Fig. 3), and $[111]_{1:1}$, $[110]_{1:1}$, and $[001]_{1:1}$ (Fig. 4), and in both cases, the energies for BV (ionic) model calculations and Ba–systems increase monotonically as well. The Pb–systems however, do not follow this trend and $Pb(B_{1/3}, B'_{2/3})O_3$ systems depart from it more strongly than $Pb(B_{1/2}B'_{1/2})O_3$ systems. Substitution of Pb for Ba drastically reduces the ΔE-ranges, which implies that energetically favorable $Pb-O$ interactions *anticorrelate* with electrostatically favorable $B-site$ configurations. That is, an increase in the concentration of electrostatically destabilizing configurations implies an increase in the concentration of stabilizing $Pb-O$ bonds, leading to a reduced change in configurational energy for the $Pb(B_{1/3}, B'_{2/3})O_3$ systems. This trend is more pronounced in the $A(B_{1/3}, B'_{2/3})O_3$ systems than in the $A(B_{1/2}B'_{1/2})O_3$ systems because of the larger difference in $B-ion$ charges, B^{2+} and B'^{5+} vs. B^{3+} and B'^{5+}, respectively. Note that in the $[110]_{1:1}$' structure (Fig. 4) the substitution of Pb for Ba causes almost no change in $\Delta E_{[110]_{1:1}}$.

The most plausible explanation for these results is that hybridization of Pb 6s- and O 2p-states[25,28–31] stabilizes electrostatically unfavorable configurations; via enhanced (short) $Pb-O$ bonds to the otherwise underbonded oxygens in $B^{2+}-O-B^{2+}$ or $B^{3+}-O-B^{3+}$ triplets. Even if the GS has no underbonded oxygens, thermal disordering will create them along with overbonded oxygens in $B^{5+}-O-B^{5+}$ triplets. In the Ba-systems this energetic cost is not as strongly mitigated by short-range interactions so ordered phases are stable to higher temperatures and the supercell ΔE-hierarchies for Ba-systems resemble those for the BV (ionic) model. In the Pb-systems however, $Pb-O$ bonds to underbonded oxygens typically contract, and those towards overbonded oxygens elongate (symmetry permitting).

For example, in the PMN $[110]_{1:2}$ supercell two thirds of the $Pb's$ are in sites with only one $B^{2+}-O-B^{2+}$ triplet (one of 12) in configuration $Mg^{2+}-O-Mg^{2+}$. The $Pb-O$ bond to this oxygen is predicted to be only 2.38 $\AA$, whereas bonds to oxygens in the other triplets are: 2.62 $\AA$ for $Mg^{2+}-O-Nb^{5+}$, and 2.86, 3.09, and 3.36$\AA$ for the $Nb^{5+}-O-Nb^{5+}$ triplets. The remaining one third of $Pb's$ in the $[110]_{1:2}$ structure have two $Mg^{2+}-O-Mg^{2+}$ triplets (in the same $[110]_{cubic}$ plane) that compete for the short $Pb-O$ bond and the distances to oxygens in the different triplets are all about the same: 2.83 $\AA$ for $Mg^{2+}-O-Mg^{2+}$; 2.85 $\AA$ for $Mg^{2+}-O-Nb^{5+}$; 2.79'$\AA$ for $Nb^{5+}-O-Nb^{5+}$. Note that $\Delta E_{[110]_{1:1}}$ (Fig. 4) is essentially unchanged by the substitution of Pb for Ba because the $B-site$ coordination of Pb in this structure does not allow for contraction of some $Pb-O$ bonds without stretching an equal number. The importance of hybridization between O 2p- and Pb 6s-states in the ferroelectricity of $PbTiO_3$ was emphasized by Cohen[28] and Cohen and Krakauer[29]; and by Bellaiche et al.[31] and Wensell and Krakauer[32] in discussing the energetics of structural relaxation in PZN and BZN in the $[111]_{1:2}$ and $[001]_{1:2}$ structures.

Qualitatively, the BV model[25] captures the essence of cation ordering in the Ba-systems, but it fails for the Pb-systems. BV suggested that covalency of short $Pb-O$ bonds might provide a mechanism for stabilizing $1:1$ order in place of $1:2$, but no specific mechanism was described. They preferred the proposal that Pb^{4+} on $B-sites$ might be responsible for "the weak 1:1 order in PMN and PMT." This is a possible contributing factor in real samples with excess lead, but it fails to explain why, in the absence of octahedral Pb^{4+}, the ΔE-ranges for $Pb(B,B')O_3$ systems are so much smaller than those of the corresponding Ba-systems. Evidently, $Pb(B,B')O_3$ perovskites are more susceptible to $B-site$ cation disorder than their Ba-counterparts because of the near cancellation of long- and short-range

contributions to the configurational energy.

IV. CONCLUSIONS

Comparing the first principles calculations for $Ba(B,B')O_3$ and $Pb(B,B')O_3$ perovskites indicates that the long-range Coulomb interactions which drive $B-site$ ordering in $Ba-$systems do not dominate in Pb-systems. Apparently, hybridization between Pb $6s$- and O $2p$-states on otherwise *underbonded oxygens*, leads to a near cancellation of long- and short-range contributions to the configurational energies of $Pb(B_{1/3},B'_{2/3})O_3$ systems, and to a partial cancellation in the $Pb(B_{1/2}B'_{1/2})O_3$ systems. This competition between long- and short-range many-body interactions explains why $Pb(B,B')O_3$ perovskites disorder at lower temperatures than $Ba(B,B')O_3$ perovskites.

V. ACKNOWLEDGEMENTS

The author gratefully acknowledges the assistance of G. Kresse with VASP calculations; E. Cockayne was supported by a National Research Council fellowship.

REFERENCES

[1] N. Setter and L.E. Cross J. App. Phys. **51** (8) 4356 (1980).

[2] L.E. Cross, Ferroelectrics **76** 241, (1987).

[3] M.A. Akbas and P.K. Davies, *Solid State Chemistry of Inorganic Materials*, Ed. P.K. Davies, A.J. Jacofson, C.C. Torardi, T. Vanderah, Proc. **453** 483 (1997).

[4] S. Kawashima, M. Nishida, I. Ueda, and H. Ouchi J. Am Ceram. Soc. **66**(6), 421 (1983).

[5] C-C. Lee, C-C Chou, and D-S. Tsai, In press, Ferroelectrics **206-207** 293, (1998).

[6] C.A. Randall and A.S. Bhalla, Japn. J. Appl. Phys. 29(2), 327 (1990).

[7] H.B. Krause, J.M. Cowley and J. Wheatley, Acta. Cryst. **A35** 1015- (1979).

[8] J. Chen, H.M. Chan, and M. Harmer, J. Am Ceram. Soc. **72**[**4**], 593 (1989).

[9] "The Columbite route is not successful in eliminating pyrochlore formation in $Pb(Zn_{1/3}Ta_{2/3})O_3$," J. Chen, Ph.D thesis (1991).

[10] M.A. Akbas and P.K. Davies J. Amer. Ceram. Soc. **80**(11), 2933 (1997).

[11] U. Treiber and S. Kemmler-Sack, J. Solid State Chem., **43**, 51- (1982).

[12] K.S. Hong, I. T. Kim, and C-D. Kim, J. Am Ceram. Soc. **79**(12), 3218 (1996).

[13] R. Guo, A.S. Bhalla, and L.E. Cross J. App. Phys. **75,(9)** 4704- (1994).

[14] C.G.F. Stenger and A.J. Burggraaf, Phys. Stat. Solid. **A61** 275 (1980).

[15] A. Kania, G.E. Kugel, K. Roleder, and M. Pawelczyk Ferroelectrics **125** 489 (1992). Also, A. Kania, K. Roleder, G.E. Kugel and M. Hafid Ferroelectrics **135** 75 (1992).

[16] N. Yasuda, H. Ohwa, J. Oohashi, K. Nomura, H. Terauchi, M. Iwata, and Y. Ishibashi J. Phys. Soc. Japan **67**(11) 3952 (1998).

[17] A. Kania, and M. Pawelczyk Ferroelectrics **124** 261 (1991).

[18] A.A. Bokov, I.P. Rayevsky, V.V. Neprin and V.G. Smotrakov Ferroelectrics **124** 271 (1991).

[19] V.S. Filip'ev and E.G. Fesenko Soviet Phys. Crystal. **10**[5] 532- (1966).

[20] F.S. Galasso and W. Darby J. Chem. Phys. **66** 131 (1962). Also, F.S. Galasso **Structure, Properties and Preparation of Perovskite type Compounds** Pergamon Press (1969).

[21] L. Brixner J. Chem. Phys. **64** 165 (1960).

[22] G.G. Jones, C.A. Randall, S.J. Jang, and T.R. Shrout Ferroelectrics

[23] G. Kresse and J. Hafner, Phys. Rev. B **47**, 558 (1993); G. Kresse, Thesis, Technische Universität Wien 1993; Phys. Rev. B **49**, 14 251 (1994). G. Kresse and J. Furthmüller, Comput. Mat. Sci. **6**, 15 (1996); Phys. Rev. **54**, 11169 (1996); cf. http://tph.tuwien.ac.at/ vasp/guide/vasp.html.

[24] D. Vanderbilt, Phys. Rev. **B41** 7892, (1990).

[25] L. Bellaiche and D. Vanderbilt, PRL **81**, 1318 (1998).

[26] For $A(B_{1/3}B'_{2/3})O_3$ systems $a = 7.7\ a.u.$ and $\epsilon = 10$ as in BV. For $A(B_{1/3}B'_{2/3})O_3$ systems $\epsilon = 5$ so that $\Delta E_{[001]_{1:1}} \approx E(BSN)_{[001]_{1:1}} \approx E(BST)_{[001]_{1:1}}$.

[27] B.P. Burton, in press, J. Phys. Chem. Solids (1999).

[28] R. E. Cohen Nature **358**, 136 (1992).

[29] R. E. Cohen and H. Krakauer, Ferroelectrics **136**, 65 (1992).

[30] L. F. Mattheiss, Phys. Rev. **B6**, 4718 (1972).

[31] L. Bellaiche, J. Padilla and D. Vanderbilt, PRB **59** 1834 (1999).

[32] M. Wensell and H. Krakauer, in press, J. Phys. Chem. Solids (1999).

TABLES

TABLE I. Experimental data on ordering in $A(B,B')O_3$ perovskites.

System	abbreviation	Observed Ordering	Transition Temperature Range	Ref.
$Pb(Zn_{1/3},Nb_{2/3})O_3$	PZN	$1:1$ Short Range Order		[6]
$Pb(Mg_{1/3},Nb_{2/3})O_3$	PMN	$1:1$ Short Range Order		[7,8]
$Pb(Zn_{1/3},Ta_{2/3})O_3$	PZT	?		[9]
$Pb(Mg_{1/3},Ta_{2/3})O_3$	PMT	1:1 $\rightleftharpoons$ Disordered	$1350 < T_t^* < 1400°C$	[10]
$Ba(Zn_{1/3},Nb_{2/3})O_3$	BZN	1:2 $\rightleftharpoons$ Disordered	$1300 < T_t < 1350°C$	[11,12]
$Ba(Mg_{1/3},Nb_{2/3})O_3$	BMN	1:2 $\rightleftharpoons$ Disordered	$1350 < T_t < 1400°C$	[10]
$Ba(Zn_{1/3},Ta_{2/3})O_3$	BZT	1:2 $\rightleftharpoons$ Disordered	$T_t \geq 1650°C$	[4]
$Ba(Mg_{1/3},Ta_{2/3})O_3$	BMT	1:2 $\rightleftharpoons$ Disordered	$T_t \approx 1655°C$	[13]
$Pb(Sc_{1/2},Nb_{1/2})O_3$	PSN	1:1 $\rightleftharpoons$ Disordered	$1200 < T_t < 1220°C$	[14]
$Pb(Sc_{1/2},Ta_{1/2})O_3$	PST	1:1 $\rightleftharpoons$ Disordered	$1350 < T_t < 1400°C$	[10]
$Pb(In_{1/2},Nb_{1/2})O_3$	PIN	1:1 $\rightleftharpoons$ Disordered	$920°C < T_t < 950°C$	[15,16]
$Pb(In_{1/2},Ta_{1/2})O_3$	PIT	1:1 $\rightleftharpoons$ Disordered	$1070°C < T_t < 1100°C$	[17,18]
$Ba(Sc_{1/2},Nb_{1/2})O_3$	BSN	1:1 $\rightleftharpoons$ Disordered	$1400°C < T_t$	[19]
$Ba(Sc_{1/2},Ta_{1/2})O_3$	BST	1:1 $\rightleftharpoons$ Disordered	$1400°C < T_t$	[19]
$Ba(In_{1/2},Nb_{1/2})O_3$	BIN	1:1	$1200°C < T_t < 1400°C$	[20,21]
$Ba(In_{1/2},Ta_{1/2})O_3$	BIT	1:1	$1200°C < T_t < 1650°C$	[20,22]

*T_t = *cation order − disorder transition temperature.*

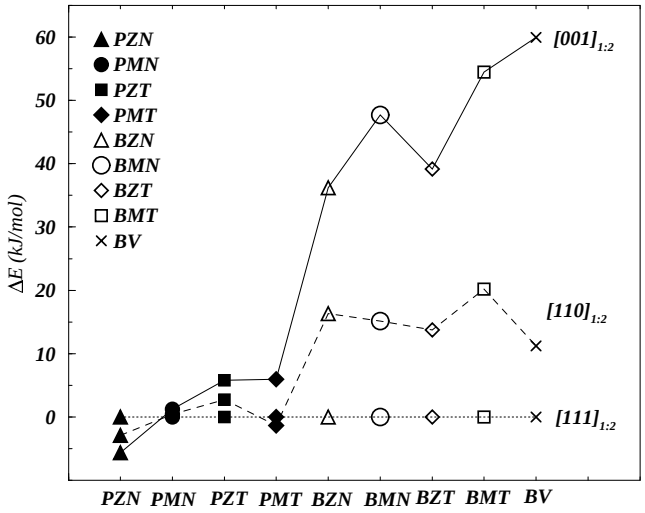

FIG. 1. Total energies (mol = ABO_3), relative to $E_{[111]_{1:2}}$, for the perovskite based supercells with compositions $A(B_{1/3}B'_{2/3})O_3$; $A = Pb, Ba$; $B = Mg, Zn$; $B' = Nb, Ta$; and for ionic model of Bellaiche and Vanderbilt (BV)[18].

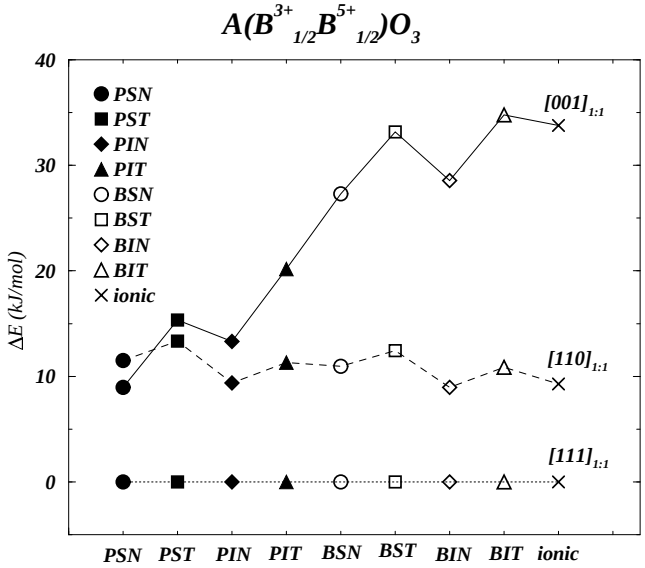

FIG. 2. Total energies, relative to $E_{[111]_{1:1}}$, for $A(B_{1/2}B'_{1/2})O_3$ perovskite based supercells.

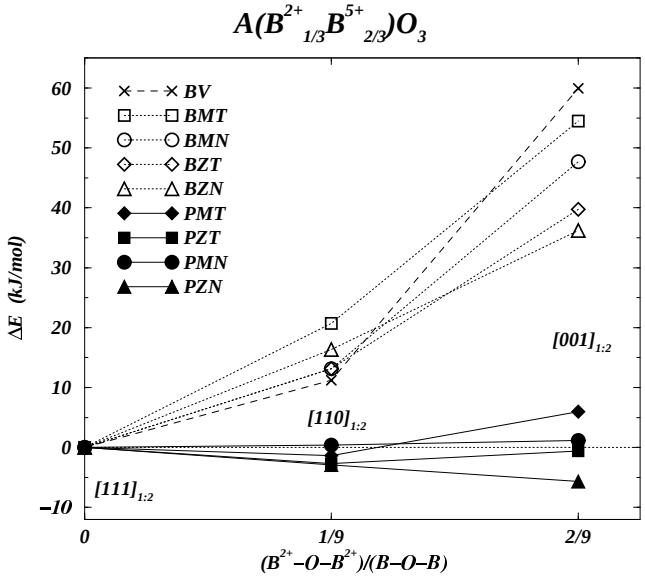

FIG. 3. ΔE vs. the concentration of underbonded oxygens in the $[111]_{1:2}$, $[110]_{1:2}$, and $[001]_{1:2}$ supercells.

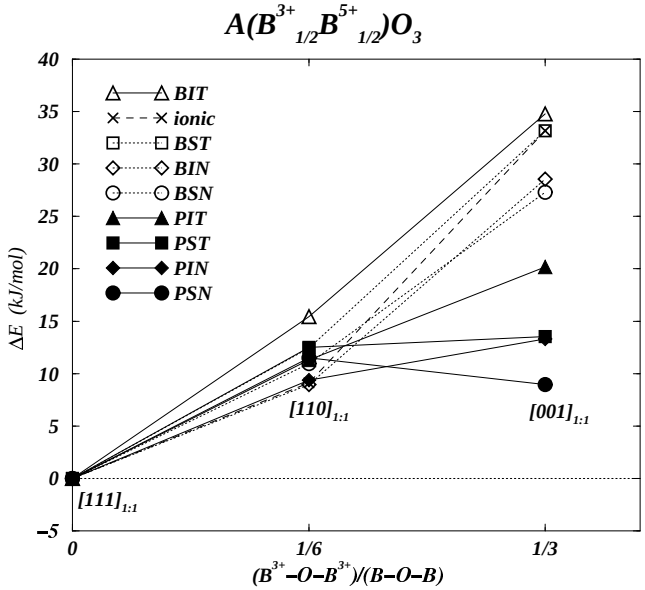

FIG. 4. ΔE vs. the concentration of underbonded oxygens in the $[111]_{1:1}$, $[110]_{1:1}$, and $[001]_{1:1}$ supercells.